DOI 10.1007/s11094-022-02639-6
Pharmaceutical Chemistry Journal, Vol. 56, No. 3, June, 2022 (Russian Original Vol. 56, No. 3, March, 2022)

STRUCTURE-BASED DESIGN AND STRUCTURE-ACTIVITY RELATIONSHIP ANALYSIS OF SMALL MOLECULES INHIBITING BCL-2 FAMILY MEMBERS

Tong Ji,[1] Boris A. Margulis,[2] Ziqian Wang,[1,*] Ting Song,[1] Yafei Guo,[3] Hao Pan,[1] and Zhichao Zhang[1,*]

Original article submitted March 20, 2021.

Based on a Mcl-1/Bcl-2 dual inhibitor **(S1)** previously reported by our group, structure-directed molecular design and structure-activity relationship (SAR) analysis were performed to investigate structural features contributing to the Mcl-1/Bcl-2 binding selectivity and affinity. A series of **S1** derivatives with various pharmacophores were synthesized, and among these a selective Mcl-1 inhibitor **A4** with 5-fold selectivity over Bcl-2 (K_i = 0.37 ± 0.07 μM vs. 1.87 ± 0.21 μM) and a dual Mcl-1/Bcl-2 inhibitor **B3** with optimized affinities (K_i = 0.35 ± 0.01 μM for Mcl-1 and 0.81 ± 0.01 μM for Bcl-2) were revealed by fluorescence polarization assay (FPA). The SAR data and binding modes of **A4** and **B3** examined by molecular docking showed that the p1 pocket having different geometry and binding features between Mcl-1 and Bcl-2 contributed to the specific binding properties of Mcl-1, and the spatial conserved N223 on Mcl-1 and N143 on Bcl-2 were the key residues to form additional hydrogen bonds with the ester of **B3**. Finally, the apoptosis-inducing potencies of **A4** and **B3** in the μM range against K562 and MCF-7 cancer cells were consistent with their binding selectivity determined *in vitro*, and only weak killing was found for these compounds in the normal cells.

Keyword: Mcl-1/Bcl-2 dual inhibitor; selective Mcl-1 inhibitor; apoptosis; anticancer activity.

1. INTRODUCTION

Members of the B-cell lymphoma-2 (Bcl-2) protein family are critical regulators of apoptosis, and the life-or-death decision is mediated primarily by the BH3 helix of pro-apoptotic fractions (the death effectors Bax and Bak, and BH3-only proteins) inserting into the hydrophobic BH3 groove on the surface of anti-apoptotic Bcl-2-like subfamily [1 – 5]. Thus, the BH3 groove of Bcl-2-like proteins, including Bcl-2, Mcl-1, and Bcl-xl, is the structure basis for antitumor drug development [6, 7].

A specific Bcl-2 inhibitor, ABT-199, was approved by the FDA in 2016 as a targeted antitumor drug [8 – 10]. However, its failure against Mcl-1-overexpressed tumors suggests that Mcl-1 is an alternative tumor target [11 – 13] so that Bcl-2 and Mcl-1 represent two arms of the anti-apoptosis function [14, 15]. Accordingly, a pan-Bcl-2 inhibitor that can occupy the BH3 groove of at least Bcl-2 and Mcl-1 to disarm the pro-survival capacities of these key targets may have some advantages in clinical development. The affinities of different molecules (e.g., ABT-199, ABT-737, A-1210477, AT-101, **S1**) for the BH3 groove are very different for various Bcl-2-like proteins, indicating the difference between the BH3 grooves of Bcl-2-like proteins [8, 16 – 20]. It is still a challenge to develop either pan-Bcl-2 inhibitors or specific Mcl-1 inhibitors that could be combined with ABT-199.

The BH3-only protein Bim displays a broad binding spectrum that enables it to antagonize both Bcl-2 and Mcl-1 proteins by inserting the BH3 α-helix into their BH3 grooves [21—23]. As such, a binding model with these proteins is attractive for designing small molecule pan-Bcl-2 inhibitors [24, 25]. In structural analysis of the Bim BH3 peptide in complex with Bcl-2 and Mcl-1, we found four conserved hydrophobic residues (h1–h4) on the Bim BH3 α-helix inserted into four hydrophobic pockets (p1–p4) within the BH3 grooves of both proteins [26, 27]. Based on the map of these four pockets, our group developed several series of inhibitors for Bcl-2-like proteins [28, 29]. An authentic BH3 mimetic and pan-Bcl-2 inhibitor targeting both Bcl-2 and Mcl-1,

[1] State Key Laboratory of Fine Chemicals, School of Chemistry, Dalian University of Technology, Dalian, China.
[2] Institute of Cytology RAS, Tikhoretsky av., 4, St. Petersburg, 194064 Russia.
[3] School of Life Science and Technology, Dalian University of Technology, Dalian, China.
[*] e-mail: wangziqian@dlut.edu.cn; zczhang@dlut.edu.cn

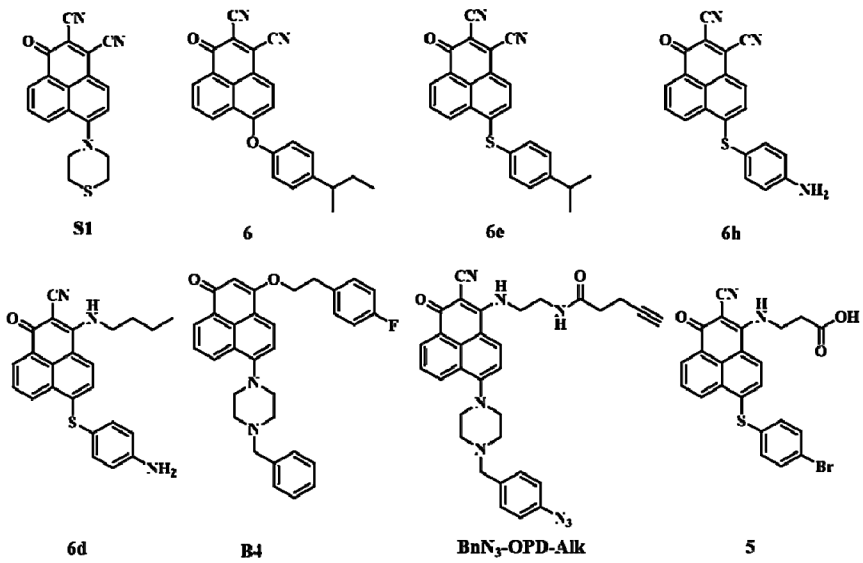

Fig. 1. Dual Mcl-1/Bcl-2 inhibitors and selective Mcl-1 inhibitor based on 2,3-dicyanophenanone framework.

6-morpholino-1-oxo-1*H*-phenalene-2,3-dicarbonitrile (**S1**) has been developed [20, 30]. In addition, many series of pan-inhibitors binding a broad spectrum of Bcl-2 family members and selective inhibitors binding only one target based on **S1** have been developed, e.g., dual inhibitors of Mcl-1 and Bcl-2 (**6**, **6e**, **6h**, **6d**, **B4**, **BnN3-OPD-Alk**) [15, 31—34] and a selective Mcl-1 inhibitor (**5**) (Fig. 1) [15]. These molecules exhibited crucial "hot-spots" and unique binding properties of both proteins for Mcl-1/Bcl-2 dual inhibitors and selective inhibitors.

In the present study, we have performed a structure-based design and synthesized a series of **S1** analogs with different pharmacophores binding either the p1 or p4 pocket on Bcl-2 and Mcl-1 surface, resulting in the selective Mcl-1 inhibitor **A4** and new dual inhibitor **B3**. In addition, we investigated in detail the binding properties of BH3 groove on the two tumor targets using SAR analysis and molecular docking studies.

2. RESULTS AND DISCUSSION

2.1 Rationale

Previously, **S1** was developed as the first authentic BH3 mimetic and a dual inhibitor of Mcl-1 and Bcl-2 (Fig, 1). The binding mode of **S1** derivatives has been identified by three-dimensional (3D) NMR. **S1** is located along a hydrophobic BH3 groove of the Mcl-1 or Bcl-2 protein surface. The carbonyl group of **S1** binds close to R263 of Mcl-1 and R146 of Bcl-2 to form a hydrogen bonded network with arginine. The thiomorpholine group of **S1** occupies the p2 pocket, and the 3-cyano group stretches toward the p4 pocket of Mcl-1 and Bcl-2.

We improved the Mcl-1/Bcl-2 dual binding of the inhibitors by further exploring p2 pockets and optimizing R1 positions of the **S1** scaffold. To gain insight into the p2 pocket of Mcl-1 and Bcl-2, we replaced the thiomorpholine of **S1** with 4-isopropylbenzenethiol to occupy the p2 pocket of Mcl-1 and Bcl-2 and obtain 6-((4-isopropylphenyl)thio)-1-oxo-1H-phenalene-2,3-dicarbonitrile (**6e**) with optimal activities (Fig. 1). Examination of **6e** and its analogs revealed that the p1 and p2 pockets of Mcl-1 are more contiguous compared with those in Bcl-2 because M231, which is located between p1 and p2 pockets of Mcl-1, is solvent exposed. The corresponding differences in the p1 and p2 pockets could contribute to the selective binding properties between Mcl-1 and Bcl-2, while the conserved R263/R146 could be the binding "hot spot" for dual inhibitors targeting both Mcl-1 and Bcl-2.

In this case, we replaced the sulfur atom with nitrogen atom at the R1-position of **6e**, resulting in the series **A** compounds (Fig. 2), in which the nitrogen atom changed the relative position of the hydrophobic group so as to orient the benzene ring into the p1 pocket. Taking advantage of the differing bond angles and alkyl-chain lengths to probe the p1 and p2 pockets, we were able to achieve selective inhibition of Bcl-2-like proteins. Then we investigated the hydrophobic pocket of p4, designed and synthesized the series **B** derivatives based on **6e** (Fig. 2), decorated at R2 position with substituents of different sizes and properties to form more favorable interactions between substituents and the p4 pocket.

2.2. Chemistry

The synthetic routes of compounds **A1**–**A4** and **B1**–**B11** are shown in Scheme 1. The initial 2,3-dicyanophenanone was synthesized according to our methods reported previously [20]. Then, 2,3-dicyanophenanone was reacted with the corresponding R_1H in CH_3CN to give **A1**–**A4**. For

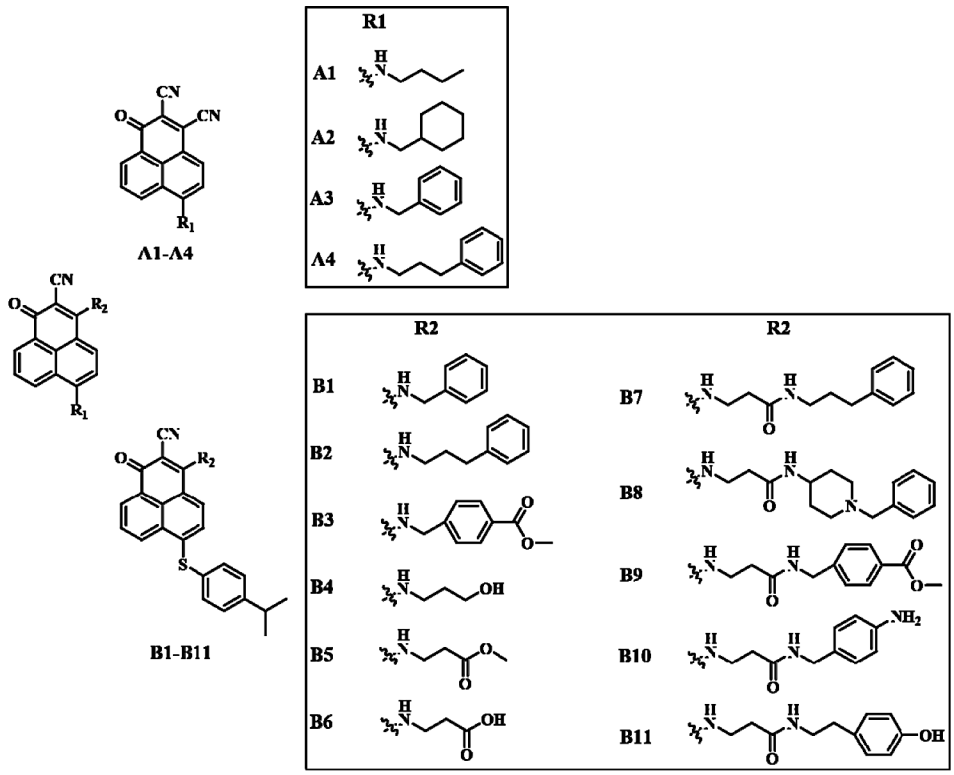

Fig. 2. Structures of compounds **A1**–**A4** and **B1**–**B11**.

B1–**B5**, 2,3-dicyanophenanone was reacted with 4-isopropylbenzenethiol to give intermediate **6e** and **6e** and then underwent S_NAr substitution with the corresponding R_2H to give the final compounds. **B6** was obtained by hydrolysis of **B5**, and then condensation between **B6** and the corresponding amine gave compounds **B7**–**B11**.

2.3. Structure-Activity Relationship

First, we substituted the thiomorpholine with amines at R1-position with different chain lengths so that they could readily reach and engage the p1 pocket. Specifically, we investigated N-butylamino-, cyclohexylmethylamino-, benzylamino-, and 3-phenylpropylamino groups yielding compounds **A1**–**A4** (Fig. 2). The binding affinities (K_i) of the compounds with Mcl-1 and Bcl-2 were evaluated by fluorescence polarization assay (FPA; Table 1). Competitive binding curves of these inhibitors to Mcl-1 and Bcl-2 are plotted in Fig. 3. The classical Mcl-1 and Bcl-2 inhibitor (-)-gossypol was used as a positive control.

Compounds **A1**–**A3** exhibited affinity to both proteins, which was maximum in **A2** (K_i = 0.65 ± 0.09 μM for Mcl-1, and K_i = 1.75 ± 0.19 μM for Bcl-2). This result indicated that **A2** occupies more space in the p1 and p2 pockets than **A1**. The affinity of **A3** was reduced for both targets, most likely due to steric hindrance by the rigid benzene ring. The significantly enhanced binding to Mcl-1 was found for **A4** (K_i = 0.37 ± 0.07 μM), which is about 4-fold higher than it to Bcl-2 (K_i = 1.87 ± 0.21 μM). As shown by the 3D docking of **A4** in complexed with Mcl-1 and Bcl-2 (Figs. 3a and 3b), the relatively longer and flexible linker of **A4** projects the hydrophobic benzene ring to occupy the p1 pocket on Mcl-1 which is continuous and more open than that on Bcl-2.

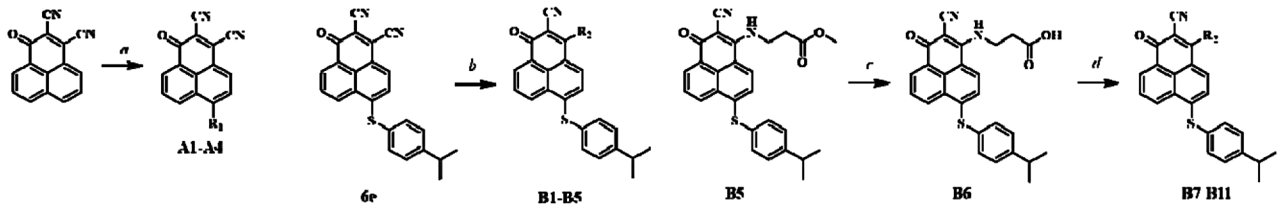

Scheme 1. Synthesis routes of compounds **A1**–**A4** and **B1**–**B11**: (*a*) H_2N-R, acetonitrile, rt, 0.5 h; (*b*) H_2N-R, acetonitrile, rt, 0.5 h; (*c*) NaOH, H_2O, tetrahydrofuran, rt, 12 h; (*d*) H_2N-R, HATU, DIEA/DBU, acetonitrile, rt, 18 h.

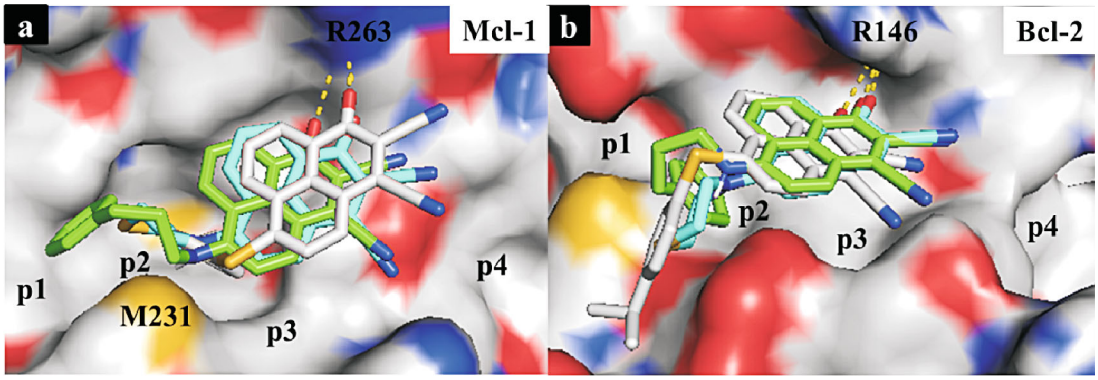

Fig. 3. Predicted binding models of **S1** (cyan), **A4** (green) and **6e** (white) in complexes with (a) Mcl-1 and (b) Bcl-2 (PDB ID: 2NLA for Mcl-1 and 1GJH for Bcl-2). Hydrogen, oxygen, sulfur, and nitrogen atoms are colored white, red, yellow, and blue, respectively. Hydrogen bonds are shown as dotted lines in yellow.

Although the activities of series **A** compounds are no better than those of **6e** because the benzene ring at R1 has been replaced (resulting in the loss of hydrophobic interactions with the p2 pocket), the series A compounds (with the sulfur atom replaced by nitrogen to align an increased steric bulk of the R1 substituents with the p1 pocket) provide insight into the pocket-volume difference of the p1 pocket in both Mcl-1 and Bcl-2.

TABLE 1. Binding Affinities (by FPA) of Compounds **A** and **B** to Mcl-1/Bcl-2

Compound	R_1	R_2	FPA [$K_i \pm$ SD (iM)][b]	
			Mcl-1	Bcl-2
(-)-Gossypol [a]	–	–	0.21 ± 0.02	0.43 ± 0.06
A1	$C_4H_{10}N$	CN	1.19 ± 0.12	3.55 ± 1.09
A2	$C_7H_{14}N$	CN	0.65 ± 0.09	1.75 ± 0.19
A3	C_7H_8N	CN	<50%, [10 μM]	2.70 ± 0.35
A4	$C_9H_{12}N$	CN	0.37 ± 0.07	1.87 ± 0.21
B1	$C_9H_{11}S$	C_7H_8N	0.59 ± 0.05	2.12 ± 0.22
B2	$C_9H_{11}S$	$C_9H_{12}N$	0.52 ± 0.09	1.28 ± 0.13
B3	$C_9H_{11}S$	$C_9H_{10}NO_2$	0.35 ± 0.01	0.81 ± 0.01
B4	$C_9H_{11}S$	C_3H_8NO	0.70 ± 0.05	1.46 ± 0.17
B5	$C_9H_{11}S$	$C_4H_8NO_2$	1.08 ± 0.04	1.98 ± 0.57
B6	$C_9H_{11}S$	$C_3H_6NO_2$	1.07 ± 0.01	<50%, [10 μM]
B7	$C_9H_{11}S$	$C_{12}H_{17}N_2O$	1.08 ± 0.02	2.52 ± 0.02
B8	$C_9H_{11}S$	$C_{15}H_{22}N_3O$	1.06 ± 0.02	0.80 ± 0.01
B9	$C_9H_{11}S$	$C_{12}H_{15}N_2O_3$	1.08 ± 0.01	1.28 ± 0.40
B10	$C_9H_{11}S$	$C_{10}H_{14}N_3O$	<50%, [10 μM]	<50%, [10 μM]
B11	$C_9H_{11}S$	$C_{11}H_{15}N_2O_2$	<50%, [10 μM]	<50%, [10 μM]

[a] (-)-Gossypol was obtained from Selleck, China.
[b] Values are the mean ± standard deviation of three independent experiments.

Next, we chose **6e** as the initial model in which R2 groups were substituted with gradual growth in the steric bulk to occupy the hydrophobic p4 pocket to further modify dual inhibition and probe the p4 pocket showing significant binding differences between Mcl-1 and Bcl-2, resulting in **B1**–**B11**. The binding affinity of **B1** ($K_i = 0.59 \pm 0.05$ μM) and **B2** ($K_i = 0.52 \pm 0.09$ μM) to Mcl-1 was approximately 2-fold higher than **B7** ($K_i = 1.08 \pm 0.02$ μM) and **B8** ($K_i = 1.06 \pm 0.02$ μM), but the affinity of **B8** to Bcl-2 (Ki = 0.80 ± 0.01 μM) was about 2-fold higher than **B1** ($K_i = 2.12 \pm 0.22$ μM), **B2** ($K_i = 1.28 \pm 0.13$ μM) and **B7** ($K_i = 2.52 \pm 0.02$ μM). According to the binding modes predicted by docking, we found that the shallow p4 pocket of Mcl-1 favors **B1** and **B2** with a linker of 1 to 3 carbons more than **B7** and **B8** with longer linker (Fig. 4*a*). It is most likely due to the solvent-exposure effect. In contrast, the longest linker of **B8** extends deeper into the p4 pocket of Bcl-2 at an appropriate angle, as the carbon atom of **B7** has been replaced by a nitrogen atom, and provides an additional hydrophobic interaction, revealing a deeper and more spacious p4 pocket (Fig. 4*b*). Taken together, the p4 pocket of Mcl-1 is not as tolerant as that of Bcl-2.

Compared with **B1** and **B9**, the binding affinity of **B3** to both Mcl-1 ($K_i = 0.35 \pm 0.01$ μM) and Bcl-2 ($K_i = 0.81 \pm 0.01$ μM) was enhanced. Molecular docking study showed that a 4.0 Å long hydrogen bond was formed between the ester group of **B3** and N223 on the α2-helix of Mcl-1 and a 3.6 Å long hydrogen bond with N143 on the other side of BH3 groove of Bcl-2 (cf. Figs. 5a and 5b) explaining the enhanced affinity.

Significant affinity shrinkage was found for **B10** and **B11**, which showed less than 50% inhibition at 10 μM, prob-

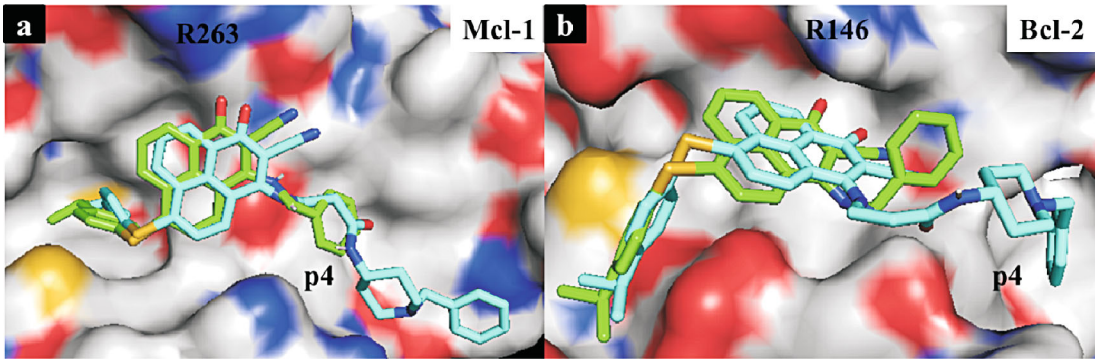

Fig. 4. Predicted binding models of **B1** (green) and **B8** (cyan) in complexes with (a) Mcl-1 and (b) Bcl-2 (PDB ID: 2NLA for Mcl-1 and 1GJH for Bcl-2). Hydrogen, oxygen, sulfur, and nitrogen atoms are colored white, red, yellow, and blue, respectively.

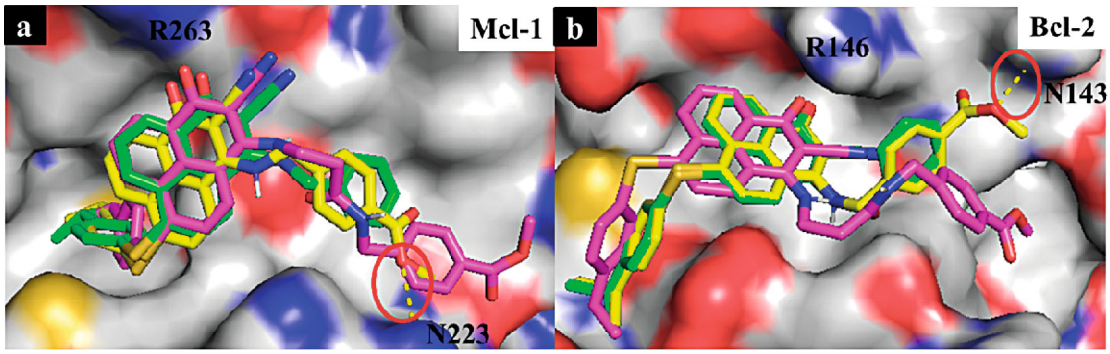

Fig. 5. Predicted binding models of **B1** (green), **B3** (yellow) and **B9** (magenta) in complexes with (a) Mcl-1 and (b) Bcl-2 (PDB ID: 2NLA for Mcl-1 and 1GJH for Bcl-2). Hydrogen, oxygen, sulfur, and nitrogen atoms are colored white, red, yellow, and blue, respectively. Hydrogen bonds are shown as dashed lines in yellow and labeled in the red cycle.

ably due to the solvent-exposing effect produced by the hydrophilic group that cannot be taken up by p4 pocket of either protein. Interestingly, although compound **B6** exhibited affinity for Mcl-1 ($K_i = 1.07 \pm 0.01$ μM), it resulted in remarkable decrease in the binding affinity for Bcl-2 (<50% inhibition at 10 μM). The carboxyl group of **B6** was found to be able to form a salt bridge with H224 of Mcl-1, but to coincide with Y108 of Bcl-2 due to repulsive electrostatic interactions, as predicted by docking studies (Figure 6). As expected, the affinities of **B4** ($K_i = 1.46 \pm 0.17$ μM) and **B5** ($K_i = 1.98 \pm 0.57$ μM) to Bcl-2 were significantly enhanced as a result of the attenuation of repulsion when the carboxyl group was replaced by the hydroxyl group or the ester group.

2.4. Biological Activity

According to their activities on Bcl-2 family proteins, **A4** and **B3** (the most potent compounds in the two series) were examined for their cytotoxic activities on cancer cells: K562 cells live in dependence on Mcl-1 protein, and MCF-7 cells dependent on both Mcl-1 and Bcl-2. The cells were incubated with a gradient concentration of **A4** or **B3** for 48 h, and

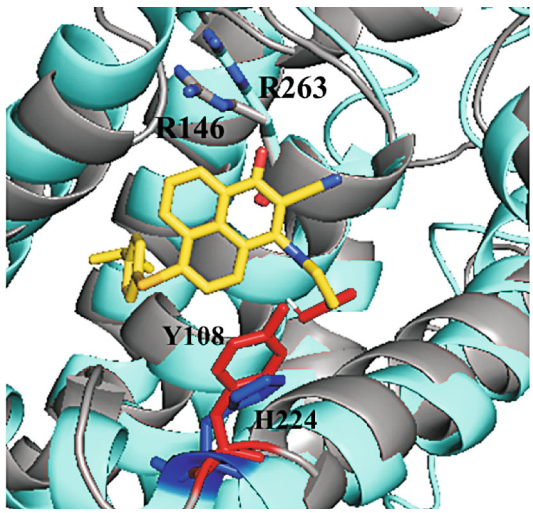

Fig. 6. Predicted binding models of **B6** (yellow) in complex with Mcl-1 (cyan) and Bcl-2(gray) (PDB ID: 2NLA for Mcl-1 and 1GJH for Bcl-2). The side chains of H224 and Y108 are shown in blue and red, respectively. The carboxyl group is shown in red. R263 (cyan) and R146 (gray) are shown with sticks. Hydrogen, oxygen, sulfur, and nitrogen atoms are colored white, red, yellow, and blue, respectively.

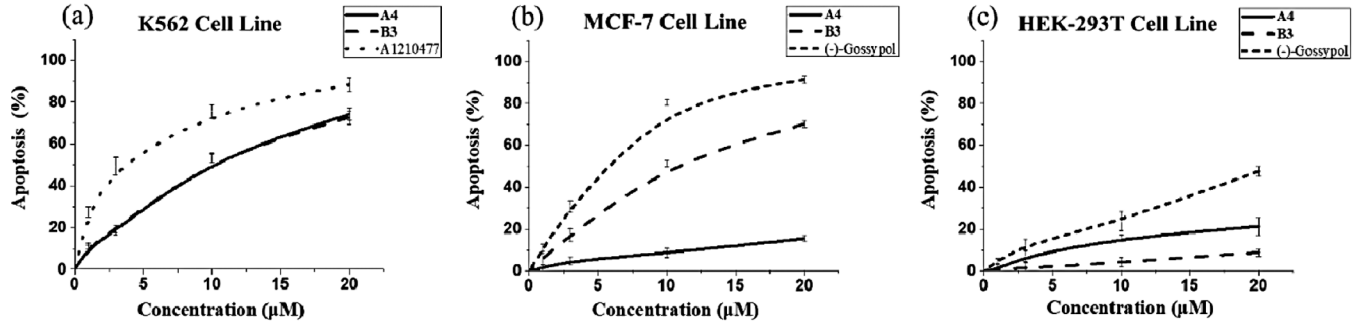

Fig. 7. Cell apoptosis of (a) K562 cells after treatment with **A4**, **B3** and A1210477, (b) MCF-7 cells after treatment with **A4**, **B3** and (-)-Gossypol, and (c) HEK-293T cells after treatment with **A4**, **B3** and (-)-gossypol as determined by Annexin-V staining assay.

then apoptosis was determined by the Annexin-V staining assay (Fig. 7). The Mcl-1 inhibitor A-1210477 in the K562 cell line and Mcl-1/Bcl-2 dual inhibitor (-)-gossypol in the MCF-7 cell line were used as positive reference, respectively.

The killing activity of **A4** in K562 cells (IC_{50} = 9.21 ± 1.08 μM) was stronger than that observed in MCF-7 cells (IC_{50} > 20 μM), consistent with binding affinity *in vitro*. Consistent with dual Mcl-1/Bcl-2 inhibition, **B3** potently induced apoptosis in both K562 cell line (IC_{50} = 7.62 ± 0.75 μM) and MCF-7 cell line (IC_{50} = 10.39 ± 0.29 μM). Both **A4** and **B3** showed weak cytotoxicity in the normal HEK-293T cell line (IC_{50} > 20 μM).

3. CONCLUSION

In summary, the molecule **B3** formed hydrogen bonds with N223 on Mcl-1 and N146 on Bcl-2, respectively. In addition, compounds **A4** and **B3** can convert their *in vitro* binding affinities and selectivity for apoptosis induction against cancer cells K562 and MCF-7 with IC_{50} values in the micromolar range.

4. EXPERIMENTAL

4.1. General

Reagents and instruments. All commercial reagents were purchased and used without further purification. The ^{1}H NMR and ^{13}C NMR were recorded using Bruker AV-400 and Bruker AV-500 spectrometers with chemical shifts reported as δ (ppm) with the multiplicity of signals indicated as follows: s, singlet; d, doublet; t, triplet; q, quartet; m, multiplet. High resolution mass spectra (HRMS) were obtained using LC/Q-TOF-MS instrument.

4.2. Chemical Synthesis

4-Thiomorpholinyl-2,3-dicyanophenanone (compound **S1)** was prepared as described previously [20].

6-((4-isopropylphenyl)thio)-1-oxo-1H-phenalene-2,3-dicarbonitrile (compound **6e)** was prepared as described previously [32].

General procedure for the synthesis of compounds A1–A4. 2,3-Dicyanophenanone (230 mg, 1.0 mmol) was stirred with various amines (20.0 mmol) in CH_3CN (20 mL) at room temperature (rt) for 0.5 h. After evaporation under reduced pressure, the product was purified by column chromatography on silica gel (CH_2Cl_2/EA, 10:1).

6-(Butylamino)-1-oxo-1H-phenalene-2,3-dicarbonitrile (A1): purple solid, yield: 30%. ^{1}H NMR (500 MHz, DMSO-d_6) δ 9.65 (s, 1H), 8.98 (d, *J* = 8.1, 1.2 Hz, 1H), 8.64 (d, *J* = 7.7, 1.1 Hz, 1H), 8.04 (d, *J* = 9.1 Hz, 1H), 7.94 (t, *J* = 7.9 Hz, 1H), 7.08 (d, *J* = 9.2 Hz, 1H), 3.61 (t, *J* = 7.2 Hz, 2H), 1.77 – 1.69 (m, 2H), 1.48 – 1.40 (m, 2H), 0.96 (t, *J* = 7.4 Hz, 3H). ^{13}C-NMR (100 MHz, DMSO-d_6): δ 175.2, 148.5, 139.9, 131.7, 131.6, 131.4, 127.5, 126.9, 125.1, 123.0, 120.4, 118.8, 118.2, 115.8, 109.8, 51.4, 26.0, 20.1, 13.8. ESI-MS: m/z $C_{19}H_{15}N_3O$, $[M+H]^+$ calculated 302.1288, found 302.1290.

6-((Cyclohexylmethyl)amino)-1-oxo-1H-phenalene-2,3-dicarbonitrile (A2): purple solid, yield: 25%. ^{1}H NMR (500 MHz, DMSO-d_6) δ 9.67 (s, 1H), 8.98 (d, *J* = 8.1 Hz, 1H), 8.61 (d, *J* = 7.6 Hz, 1H), 7.98 (d, *J* = 9.0 Hz, 1H), 7.91 (t, *J* = 7.9 Hz, 1H), 7.07 (d, *J* = 9.1 Hz, 1H), 3.45 (d, *J* = 6.5 Hz, 2H), 1.87 – 1.60 (m, 5H), 1.29 – 1.00 (m, 6H). ^{13}C-NMR (100 MHz, DMSO-d_6): δ 176.2, 148.5, 139.9, 131.7, 131.6, 131.4, 127.5, 126.8, 125.2, 123.0, 120.4, 118.8, 118.2, 115.8, 108.3, 49.8, 36.8, 30.5, 25.9, 25.3. ESI-MS: m/z $C_{22}H_{19}N_3O$, $[M+H]^+$ calculated 342.1601, found 342.1603.

6-(Benzylamino)-1-oxo-1H-phenalene-2,3-dicarbonitrile (A3): purple solid, yield: 17%. ^{1}H NMR (500 MHz, DMSO-d_6) δ 10.16 (s, 1H), 9.07 (d, *J* = 8.1 Hz, 1H), 8.68 (d, *J* = 7.6 Hz, 1H), 8.03 (d, *J* = 9.0 Hz, 1H), 7.99 (t, *J* = 7.9 Hz, 1H), 7.46 – 7.28 (m, 5H), 7.02 (d, *J* = 9.1 Hz, 1H), 4.87 (s, 2H). ^{13}C-NMR (100 MHz, DMSO-d_6): δ 175.2, 139.9, 137.8, 131.7, 131.6, 131.4, 128.5, 127.5, 126.9, 126.7, 125.1, 123.0, 120.4, 118.8, 118.2, 115.8, 109.8, 48.4. ESI-MS: m/z $C_{22}H_{13}N_3O$, $[M+H]^+$ calculated 336.1131, found 336.1135.

1-Oxo-6-((3-phenylpropyl)amino)-1H-phenalene-2,3-dicarbonitrile (A4): purple solid, yield: 20%. ^{1}H NMR (500 MHz, DMSO-d_6) δ 9.66 (s, 1H), 8.97 (d, J = 8.1 Hz, 1H), 8.64 (d, J = 7.6 Hz, 1H), 8.03 (d, J = 9.1 Hz, 1H), 7.94 (t, J = 7.9 Hz, 1H), 7.32 – 7.16 (m, 5H), 7.04 (d, J = 9.1 Hz, 1H), 3.63 (t, J = 7.3 Hz, 2H), 2.76 (t, J = 7.7 Hz, 2H), 2.10 – 2.02 (m, 2H). ^{13}C-NMR (100 MHz, DMSO-d_6): δ 175.2, 148.5, 142.0, 139.9, 131.7, 131.6, 131.4,128.8, 128.1, 127.5, 126.9, 126.0, 125.1, 123.0, 120.4, 118.8, 118.2, 115.8, 109.8, 45.0, 30.7, 29.1. ESI-MS: m/z $C_{24}H_{17}N_3O$, $[M+H]^+$ calculated 364.1444, found 364.1448.

General procedure for the synthesis of compounds B1–B5. A mixture of compound **6e** (114 mg, 0.3 mmol) and amines with different substituent groups stirred in CH_3CN (20mL) at rt for 0.5 h. The resulting mixture was concentrated and the crude was purified on silica gel (CH_2Cl_2/MeOH 30:1).

3-(Benzylamino)-6-((4-isopropylphenyl)thio)-1-oxo-1H-phenalene-2-carbonitrile (B1): yellow solid, yield: 22%. ^{1}H NMR (500 MHz, Chloroform-*d*) δ 8.50 (d, J = 7.3 Hz, 1H), 8.45 (d, J = 8.3 Hz, 1H), 7.63 (t, J = 7.8 Hz, 1H), 7.45 (d, J = 8.3 Hz, 1H), 7.35 (d, J = 7.8 Hz, 2H), 7.30 – 7.11 (m, 7H), 6.86 (d, J = 8.1 Hz, 1H), 5.81 (s, 1H), 5.05 (d, J = 4.8 Hz, 2H), 2.88 – 2.78 (m, 1H), 1.14 (d, J = 7.1 Hz, 6H). ^{13}C-NMR (100 MHz, Chloroform-*d*): δ 178.1, 175.2, 146.9, 138.6, 137.9, 134.8, 132.9, 132.1, 131.9, 131.7, 131.4, 130.9, 128.8, 128.5, 128.2, 126.9, 126.7, 126.0, 125.1, 115.8, 78.2, 47.6, 33.2, 23.2. ESI-MS: m/z $C_{30}H_{24}N_2OS$, $[M+H]^+$ calculated 461.1682, found 461.1688.

6-((4-Isopropylphenyl)thio)-1-oxo-3-((3-phenylpropyl)-amino)-1H-phenalene-2-carbonitrile (B2): yellow solid, yield: 25%. ^{1}H NMR (500 MHz, DMSO-d_6) δ 8.60 (d, J = 8.3 Hz, 2H), 8.45 (d, J = 7.3 Hz, 1H), 8.38 (d, J = 8.3 Hz, 1H), 7.88 (d, J = 7.8 Hz, 1H), 7.49 (d, J = 8.2 Hz, 2H), 7.39 (d, J = 8.2 Hz, 2H), 7.29 – 7.19 (m, 5H), 7.16 (d, J = 7.0 Hz, 1H), 3.89 (q, J = 6.9 Hz, 2H), 3.00 – 2.91 (m, 1H), 2.71 (t, J = 7.8 Hz, 2H), 2.10 – 2.02 (m, 2H), 1.23 (d, J = 6.9 Hz, 6H). ^{13}C-NMR (100 MHz, DMSO-d_6): δ 178.1, 175.2, 146.9, 142.0, 138.6, 134.8, 132.9, 132.1, 131.9, 131.7, 131.4, 130.9, 128.8, 128.2, 128.1, 126.7, 126.0, 125.1, 115.8, 78.2, 42.9, 33.2, 30.8, 29.9, 23.2. ESI-MS: m/z $C_{32}H_{28}N_2OS$, $[M+H]^+$ calculated 489.1995, found 489.1999.

Methyl-(((2-cyano-6-((4-isopropylphenyl)thio)-1-oxo-1H-phenalen-3-yl)amino)methyl)-benzoate (B3): yellow solid, yield: 23%. ^{1}H NMR (500 MHz, Chloroform-*d*) δ 8.59 (t, J = 7.7 Hz, 2H), 8.02 (d, J = 8.3 Hz, 2H), 7.75 (d, J = 7.8 Hz, 1H), 7.67 (d, J = 8.3 Hz, 1H), 7.48 (d, J = 8.2 Hz, 2H), 7.45 (d, J = 8.2 Hz, 2H), 7.32 (d, J = 8.2 Hz, 2H), 7.00 (d, J = 8.2 Hz, 1H), 6.13 (t, J = 5.4 Hz, 1H), 5.23 (d, J = 5.2 Hz, 2H), 3.90 (s, 3H), 3.01 – 2.92 (m, 1H), 1.28 (d, J = 6.9 Hz, 6H). ^{13}C-NMR (100 MHz, DMSO-d_6): δ 178.1, 175.2, 165.9, 146.9, 142.2, 138.6, 134.8, 132.9, 132.1, 131.9, 131.7, 131.4, 130.9, 129.7, 128.8, 128.2, 128.1, 126.8, 126.7, 126.0, 125.1, 115.8, 78.2, 51.5, 47.6, 33.2, 23.2. ESI-MS: m/z $C_{32}H_{26}N_2O_3S$, $[M+Na]^+$ calculated 541.1556, found 541.1558.

3-((3-Hydroxypropyl)amino)-6-((4-isopropylphenyl)-thio)-1-oxo-1H-phenalene-2-carbonitrile (B4): yellow solid, yield: 20%. ^{1}H NMR (400 MHz, Chloroform-*d*) δ 8.48 (d, J = 7.8 Hz, 2H), 7.85 (s, 1H), 7.65 (t, J = 7.8 Hz, 1H), 7.53 (d, J = 8.3 Hz, 1H), 7.48 (d, J = 8.2 Hz, 2H), 7.34 (d, J = 8.1 Hz, 2H), 6.86 (d, J = 8.2 Hz, 1H), 4.30 (q, J = 5.1 Hz, 2H), 4.13 (t, J = 5.1 Hz, 2H), 3.04 – 2.94 (m, 1H), 2.71 (s, 1H), 2.09 – 2.01 (m, 2H), 1.31 (d, J = 6.9 Hz, 6H). ^{13}C-NMR (100 MHz, Chloroform-*d*): δ 178.1, 175.2, 146.9, 138.6, 134.8, 132.9, 132.1, 131.9, 131.7, 131.4, 130.9, 128.8, 128.2, 126.7, 126.0, 125.1, 115.8, 78.2, 58.8, 39.3, 33.2, 32.9, 23.2. ESI-MS: m/z $C_{26}H_{24}N_2O_2S$, $[M+H]^+$ calculated 429.1631, found 429.1631.

Methyl 3-((2-cyano-6-((4-isopropylphenyl)thio)-1-oxo-1H-phenalen-3-yl)amino) propanoate (B5): yellow solid, yield: 30%.^{1}H NMR (500 MHz, Chloroform-*d*) δ 8.67 (d, J = 6.0 Hz, 1H), 8.60 (d, J = 7.2 Hz, 1H), 7.77 (t, J = 7.8 Hz, 1H), 7.71 (d, J = 8.2 Hz, 1H), 7.50 (d, J = 8.2 Hz, 2H), 7.35 (d, J = 8.2 Hz, 2H), 7.16 (s, 1H), 7.06 (d, J = 8.2 Hz, 1H), 4.33 (q, J = 5.9 Hz, 2H), 3.74 (s, 3H), 3.04 – 2.95 (m, 1H), 2.85 (t, J = 5.7 Hz, 2H), 1.32 (d, J = 6.9 Hz, 6H). ^{13}C-NMR (100 MHz, Chloroform-*d*): δ 178.1, 175.2, 173.1, 146.9, 138.6, 134.8, 132.9, 132.1, 131.9, 131.7, 131.4, 130.9, 128.8, 128.2, 126.7, 126.0, 125.1, 115.8, 78.2, 51.9, 33.2, 32.7, 23.2. ESI-MS: m/z $C_{27}H_{24}N_2O_3S$, $[M+H]^+$ calculated 457.1580, found 457.1584.

Synthesis of 3-((2-cyano-6-((4-isopropylphenyl)thio)-1-oxo-1H-phenalen-3-yl)amino) propanoic acid (B6). Compound **B5** (80 mg, 0.18 mmol), NaOH (114 mg, 3.6 mmol) dissolved in water were stirred in tetrahydrofuran (10 mL) at rt for 12 h. The mixture was diluted with water (30 mL) and extracted with ethyl acetate (30 mL × 3). The combined organic layer was dried over anhydrous sodium sulfate, filtered, and concentrated under reduced pressure. The residue was purified on silica gel (CH_2Cl_2/MeOH 15:1). **B6** as yellow solid, yield: 90%.^{1}H NMR (500 MHz, DMSO-d_6) δ 12.41 (s, 1H), δ 8.60 (d, J = 8.4 Hz, 1H), 8.46 (d, J = 7.2 Hz, 1H), 8.38 (d, J = 8.2 Hz, 1H), 7.88 (t, J = 7.8 Hz, 1H), 7.49 (d, J = 8.3 Hz, 2H), 7.39 (d, J = 8.3 Hz, 2H), 7.20 (d, J = 8.1 Hz, 1H), 4.09 (q, J = 6.6 Hz, 2H), 3.01 – 2.90 (m, 1H), 2.78 (t, J = 6.9 Hz, 2H), 1.23 (d, J = 6.9 Hz, 6H). ^{13}C-NMR (100 MHz, DMSO-d_6): δ 178.1, 175.5, 175.2, 146.9, 138.6, 134.8, 132.9, 132.1, 131.9, 131.7, 131.4, 130.9, 128.8, 128.2, 126.7, 126.0, 125.1, 115.8, 78.2, 40.6, 33.2, 32.4, 23.2. ESI-MS: m/z $C_{26}H_{22}N_2O_3S$, $[M-H]^-$ calculated 441.1278, found 441.1298.

General procedure for the synthesis of compounds B7–B11. Compound **B6** (70 mg, 0.16 mmol), HATU (122 mg, 0.32 mmol) and DIEA (25 mg, 0.19 mmol) or DBU (487 mg, 3.20 mmol) were stirred in CH_3CN (10 mL). After the addition of different substituent amines (0.18 mmol), the reaction mixture was stirred at rt for 18h. The mixture was diluted with water (30 mL) and extracted with CH_2Cl_2

(30 mL × 3). The organic layers were dried with anhydrous sodium sulfate, filtered and evaporated. The crude product was purified on silica gel (CH_2Cl_2/EA 8:1).

3-((2-cyano-6-((4-isopropylphenyl)thio)-1-oxo-1H-phenalen-3-yl)amino)-N-(3-phenylpropyl) propanamide (B7): yellow solid, yield: 80%.^{1}H NMR (500 MHz, Chloroform-*d*) δ 8.60 (d, *J* = 7.6 Hz, 1H), 8.56 (d, *J* = 8.3 Hz, 1H), 8.37 (s, 1H), 7.82 (d, *J* = 8.4 Hz, 1H), 7.72 (t, *J* = 7.0 Hz, 1H), 7.49 (d, *J* = 8.2 Hz, 2H), 7.35 (d, *J* = 8.2 Hz, 2H), 7.24 – 7.12 (m, 5H), 7.03 (d, *J* = 8.2 Hz, 1H), 6.15 (s, 1H), 4.31 (t, *J* = 6.7 Hz, 2H), 3.31 (q, *J* = 6.7 Hz, 2H), 3.04 – 2.96 (m, 1H), 2.70 – 2.57 (m, 4H), 1.92 – 1.84 (m, 2H), 1.33 (d, *J* = 6.9 Hz, 6H). ^{13}C-NMR (100 MHz, Chloroform-*d*): δ 178.1, 175.6, 175.2, 146.9, 142.0, 138.6, 134.8, 132.9, 132.1, 131.9, 131.7, 131.4, 130.9, 128.8, 128.2, 128.1, 126.7, 126.0, 125.1, 115.8, 78.2, 39.9, 39.8, 37.1, 33.2, 30.4, 29.0, 23.2. ESI-MS: m/z $C_{35}H_{33}N_3O_2S$, $[M+H]^+$ calculated 560.2366, found 560.2368.

N-(1-Benzylpiperidin-4-yl)-3-((2-cyano-6-((4-isopropylphenyl)thio)-1-oxo-1H-phenalen-3-yl)amino) propanamide (B8): yellow solid, yield: 82%.^{1}H NMR (500 MHz, Chloroform-*d*) δ 8.62 (d, *J* = 7.3 Hz, 1H), 8.57 (d, *J* = 9.6 Hz, 1H), δ 8.35 (s, 1H), 7.83 (d, *J* = 8.3 Hz, 1H), 7.74 (t, *J* = 7.8 Hz, 1H), 7.49 (d, *J* = 8.2 Hz, 2H), 7.37 – 7.29 (m, 7H), 7.04 (d, *J* = 8.3 Hz, 1H), 6.14 (s, 1H), 4.32 (q, *J* = 5.6 Hz, 2H), 3.81 (s, 1H), 3.54 (s, 2H), 3.04 – 2.96 (m, 1H), 2.92 – 2.80 (m, 2H), 2.65 (t, *J* = 6.0 Hz, 2H), 2.26 – 2.06 (m, 2H), 2.03 – 1.79 (m, 4H), 1.33 (d, *J* = 6.9 Hz, 6H). ^{13}C-NMR (100 MHz, Chloroform-*d*): δ 178.1, 175.2, 173.0, 146.9, 138.6, 134.8, 132.9, 132.1, 131.9, 131.7, 131.4, 130.9, 128.8, 128.4, 128.2, 127.2, 126.7, 126.0, 125.1, 115.8, 78.2, 64.7, 51.6, 47.9, 39.8, 37.4, 33.2, 30.2, 23.2. ESI-MS: m/z $C_{38}H_{38}N_4O_2S$, $[M+H]^+$ calculated 615.2788, found 615.2792.

Methyl 4-((3-((2-cyano-6-((4-isopropylphenyl)thio)-1-oxo-1H-phenalen-3-yl) amino)propanamido) methyl)benzoate (B9): yellow solid, yield: 81%.^{1}H NMR (500 MHz, DMSO-d_6) δ 8.62 (d, *J* = 7.1 Hz, 3H), 8.47 (d, *J* = 7.3 Hz, 1H), 8.33 (d, *J* = 8.2 Hz, 1H), 7.90 (t, *J* = 7.8 Hz, 1H), 7.66 (d, *J* = 8.3 Hz, 2H), 7.47 (d, *J* = 8.3 Hz, 2H), 7.38 (d, *J* = 8.4 Hz, 2H), 7.25 (d, *J* = 8.3 Hz, 2H), 7.19 (d, *J* = 8.2 Hz, 1H), 4.32 (d, *J* = 5.9 Hz, 2H), 4.19 – 4.13 (m, 2H), 3.82 (s, 3H), 3.00 – 2.90 (m, 1H), 2.74 (t, *J* = 6.5 Hz, 2H), 1.22 (d, *J* = 6.9 Hz, 6H). ^{13}C-NMR (100 MHz, DMSO-d_6): δ 178.1, 175.2, 173.6, 165.9, 146.9, 142.2, 138.6, 134.8, 132.9, 132.1, 131.9, 131.7, 131.4, 130.9, 129.7, 128.8, 128.2, 128.1, 126.8, 126.7, 126.0, 125.1, 115.8, 78.2, 51.5, 43.6, 39.8, 37.1, 33.2, 23.2. ESI-MS: m/z $C_{35}H_{31}N_3O_4S$, $[M+H]^+$ calculated 590.2108, found 590.2110.

N-(4-Aminobenzyl)-3-((2-cyano-6-((4-isopropylphenyl)-thio)-1-oxo-1H-phenalen-3-yl)amino) propanamide (B10): yellow solid, yield: 78%.^{1}H NMR (500 MHz, DMSO-d_6) δ 8.65 (s, 1H), δ 8.61 (d, *J* = 8.4 Hz, 1H), 8.46 (d, *J* = 7.2 Hz, 1H), 8.34 (d, *J* = 8.2 Hz, 1H), 8.30 (d, *J* = 5.6 Hz, 1H), 7.89 (t, *J* = 7.8 Hz, 1H), 7.49 (d, *J* = 7.9 Hz, 2H), 7.40 (d, *J* = 8.0 Hz, 2H), 7.23 (d, *J* = 8.1 Hz, 1H), 6.83 (d, *J* = 8.0 Hz, 2H), 6.40 (d, *J* = 8.2 Hz, 2H), 4.89 (s, 2H), 4.12 (t, *J* = 6.5 Hz, 2H), 4.06 (d, *J* = 5.7 Hz, 2H), 3.00 – 2.90 (m, 1H), 2.65 (t, *J* = 6.5 Hz, 2H), 1.23 (d, *J* = 6.9 Hz, 6H). ^{13}C-NMR (100 MHz, DMSO-d_6): δ 178.1, 175.2, 173.6, 146.9, 146.4, 138.6, 134.8, 132.9, 132.1, 131.9, 131.7, 131.4, 130.9, 128.8, 128.2, 127.9, 127.7, 126.7, 126.0, 125.1, 115.8, 115.0, 78.2, 43.6, 39.8, 37.1, 33.2, 23.2. ESI-MS: m/z $C_{33}H_{30}N_4O_2S$, $[M+H]^+$ calculated 547.2162, found 547.2164.

3-((2-Cyano-6-((4-isopropylphenyl)thio)-1-oxo-1H-phenalen-3-yl)amino)-N-(4-hydroxyphenethyl) propanamide (B11): yellow solid, yield: 80%.^{1}H NMR (500 MHz, DMSO-d_6) δ 9.13 (s, 1H), δ 8.64 (t, *J* = 6.1 Hz, 1H), 8.61 (d, *J* = 7.2 Hz, 1H), 8.47 (d, *J* = 7.3 Hz, 1H), 8.35 (d, *J* = 8.3 Hz, 1H), 8.06 (t, *J* = 5.7 Hz, 1H), δ 7.89 (t, *J* = 7.8 Hz, 1H), 7.46 (d, *J* = 8.3 Hz, 2H), 7.37 (d, *J* = 8.2 Hz, 2H), 7.22 (d, *J* = 8.2 Hz, 1H), 6.90 (d, *J* = 8.4 Hz, 2H), 6.60 (d, *J* = 8.4 Hz, 2H), 4.10 (q, *J* = 6.5 Hz, 2H), 3.20 – 3.13 (m, 2H), 3.00 – 2.90 (m, 1H), 2.60 (t, *J* = 6.7 Hz, 2H), 2.48 (t, *J* = 5.0 Hz, 2H), 1.22 (d, *J* = 7.0 Hz, 6H). ^{13}C-NMR (100 MHz, DMSO-d_6): δ 178.1, 175.6, 175.2, 155.7, 146.9, 138.6, 134.8, 132.9, 132.1, 132.0, 131.9, 131.7, 131.4, 130.9, 130.2, 128.8, 128.2, 126.7, 126.0, 125.1, 115.8, 78.2, 40.6, 39.8, 37.1, 35.1, 33.2, 23.3. ESI-MS: m/z $C_{34}H_{31}N_3O_3S$, $[M-H]^-$ calculated 560.2013, found 560.2016.

4.3. Bioevaluation

Fluorescence polarization-based binding assay (FPA). FAM-Bid peptide (10 nM) and Mcl-1 protein (100 nM) or Bcl-2 protein (300 nM) were preincubated in the assay buffer (25 mM Tris, 150 mM NaCl, 0.02% NaN_3, pH 8.0), and then compounds at various concentration gradients were added. After 10 min incubation, polarization (mP) values were measured using SpectraMax M5 Detection System on a black 96-well plate. The IC_{50} values were determined by plotting the fitted curves (see supplementary Fig. S1). Saturation experiments revealed that FAM-Bid binds to Mcl-1 and Bcl-2 with K_d values of 11 and 100 nM, respectively. The K_i values of tested compounds were calculated using the equation $K_i = [I]_{50}/([L]_{50}/K_d + [P]_0/K_d + 1)$ [15].

A 21-residue Bid BH3 peptide (residues 79 – 99) bearing 6-carboxy-fluorescein succinimidyl ester fluorescence tag (FAM-Bid) was purchased from HD Biosciences (Shanghai, China). The recombinant protein of Bcl-2 and Mcl-1 was synthesized and purified from *Escherichia coli* BL21 bacteria as described in our previous study, and the FPAs assay was performed according to the published literature [28].

Cell lines. Chronic myeloid leukemia (CML) K562 line cells, human breast adenocarcinoma MCF-7 line cells, and human embryonic kidney 293T (HEK-293T) cells were obtained from the Cell Bank of the Chinese Academy of Sciences (Shanghai, China) and preserved for no longer than 6 months after resuscitation. DMEM medium containing 10%

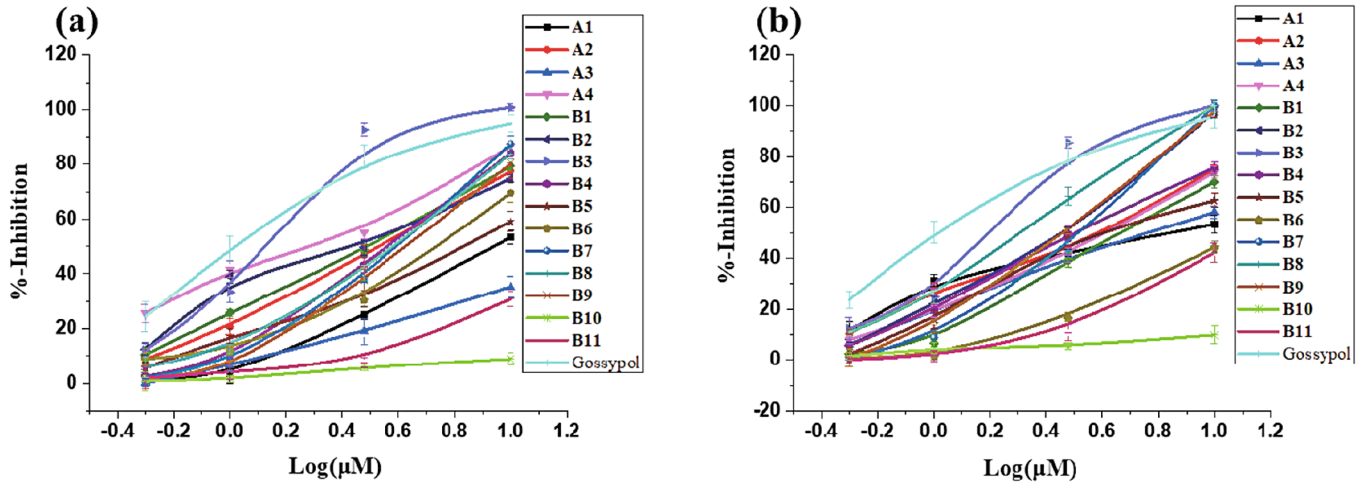

Fig. S1. Competitive binding curves of small-molecule inhibitors **A** and **B** to (a) Mcl-1 and (b) Bcl-2 as determined by FPA.

fetal bovine serum and 100 U/mL penicillin and streptomycin was used to culture the cells at 37°C under 5% CO_2 [36].

Annexin-V staining assay. Detection of apoptosis was performed using the Annexin-V apoptosis detection kit (Roche, Indianapolis, IN) according to the manufacturer's instructions. Specific experimental details can be found in our previous report [36].

4.3 Molecular Docking

The 3D structure of Mcl-1 (PDB ID: 2NLA) and Bcl-2 (PDB ID: 1GJH) was downloaded from the Protein Data Bank (PDB) and the original ligand of the pdb file was removed by PyMOL. The AutoDock 4.2 program equipped with ADT was used to perform automated molecular docking. The mol2 structures of the inhibitors were obtained using Chembio3D Ultra 11.0 followed by energy minimization. Grid maps covering residues that were perturbed more than the threshold of 0.1 ppm in the BH3 binding groove of the proteins were defined with a grid spacing of 0.375 Å for all inhibitors in the AutoDock calculations. The GA-LS algorithm was run with default parameters. For each docking job, 100 hybrid GA-LS runs were performed. A total of 100 possible binding conformations were generated and grouped into clusters based on a cluster tolerance of 1.0 Å. The docking models were analyzed and plotted using ADT.

ACKNOWLEDGEMENTS

This research was supported by the National Natural Science Foundation of China (81903462 and 82073703), the China Postdoctoral Science Foundation (2018M641694), and the Fundamental Research Funds for the Central University (DUT20LK28 and DUT20YG133).

CONFLICT OF INTEREST

The authors declare that they have no conflicts of interest.

REFERENCES

1. Kuwana, L. E. King, K. Cosentino, et al., *J. Biol. Chem*., **295**(6), 1623 – 1636 (2020).
2. E. M. Kim, C. H. Jung, J. Y. Song, et al., *Cancer Lett*., **424**, 127 – 135 (2018).
3. R. J. Youle and A. Strasser, *Nat. Rev. Mol. Cell Biol*., **9**(1), 47 – 59 (2008).
4. C. Bogner, J. Kale, J. Pogmore, et al., *Mol. Cell*., **77**(4), 901 – 912 (2020).
5. L. A. Gillies and T. Kuwana, *J. Cell. Biochem*., **115**(4), 632 – 640 (2014).
6. A. M. Hossini and J. Eberle, *Biochem. Pharmacol*., **76**(11), 1612 – 1619 (2008).
7. M. Kvansakul and M. G. Hinds, *Methods Enzymol*., **544**, 49 – 74 (2014).
8. A. J. Souers, J. D. Leverson, E. R. Boghaert, et al., *Nat. Med*., **19**(2), 202 – 208 (2013).
9. E. D. Deeks, *Drugs*, **76**(9), 979 – 987 (2016).
10. T. Song, M. Zhang, P. Liu, et al., *Biochem. Pharmacol*., **155**, 102 – 109 (2018).
11. K. Bojarczuk, B. K. Sasi, S. Gobessi, et al., *Blood*, **127**(25), 3192 – 3201 (2016).
12. S. Kehr, T. Haydn, A. Bierbrauer, et al., *Cancer Lett*., **482**, 19 – 32 (2020).
13. A. D. Blasio, R. Vento, and R. D. Fiore, *J. Cell. Physiol*., **233**(11), 8482 – 8498 (2018).
14. J. M. Eichhorn, S. E. Alford, N. Sakurikar, et al., *Exp. Cell. Res*., **322**(2), 415 – 424 (2014).
15. J. Zhu, Z. Wang, Z. Guo, et al., *Arch. Pharm*., **353**(5), e2000005 (2020).
16. J. R. Lever and E. A. Fergason-Cantrell, *Pharmacol. Res*., **142**, 87 – 100 (2019).
17. M. F. van Delft, A. H. Wei, K. D. Mason, et al., *Cancer Cell*., **10**(5), 389 – 399 (2006).

18. J. D. Leverson, H. Zhang, J. Chen, et al., *Cell Death. Dis*., **6**, e1590 (2015).
19. F. Yan, X. X. Cao, H. X. Jiang, et al., *J. Med. Chem*., **53**(15), 5502 – 5510 (2010).
20. Z. Zhang, T. Song, T. Zhang, et al., *Int. J. Cancer*, **128**(7), 1724 – 1735 (2011).
21. C. L. Day, L. Chen, S. J. Richardson, et al*., J. Biol. Chem*., **280**(6), 4738 – 4744 (2005).
22. V. V. Senichkin, A. Y. Streletskaia, B. Zhivotovsky, et al., *Trends Cell. Biol*., **29**(7), 549 – 562 (2019).
23. M. D. Boersma, H. S. Haase, K. J. Peterson-Kaufman, et al*., J. Am. Chem. Soc*., **134**(1), 315 – 323 (2012).
24. D. Merino, G. L. Kelly, G. Lessene, et al., *Cancer Cell*., **34**(6), 879 – 891 (2018).
25. S. Shukla, S. Saxena, B. K. Singh, et al., *Eur. J. Cell. Biol*., **96**(8), 728 – 738 (2017).
26. S. M. Ivanov, R. G. Huber, J. Warwicker, et al., *Structure*, **24**(11), 2024 – 2033 (2016).
27. L. Delgado-Soler, M. Pinto, K. Tanaka-Gil, et al., *J. Chem. Inf. Model*., **52**(8), 2107 – 2118 (2012).
28. Z. Zhang, P. Su, X. Li, et al., *Arch. Pharm*., **348**(2), 89 – 99 (2015).
29. Z. Wang, W. Xu, T. Song, et al., *Arch. Pharm*., **350**(1), e1600251 (2017).
30. Z. Guo, T. Song, Z. Xue, et al., *Eur. J. Pharm. Sci*., **142**, 105105 (2020).
31. Z. Zhang, H. Yang, G. Wu, et al., *Eur. J. Med. Chem*., **46**(9), 3909 – 3916 (2011).
32. Z. Zhang, G. Wu, F. Xie, et al., *J. Med. Chem*., **54**(4), 1101 – 1105 (2011).
33. T. Song, X. Li, Y. Yang, et al., *Bioorg. Med. Chem*., **22**(1), 663 – 664 (2014).
34. X. Zhang, Z. Wang, Z. Guo, et al., *Chem. Biochem*., **22**(2), 326 – 329 (2021).
35. T. Song, Z. Wang, F. Ji, et al., *Angew. Chem. Int. Ed. Engl*., **55**(46), 14250 – 14256 (2016).
36. N. He, P. Liu, Z. Wang, et al., *Biochem. Biophys. Res. Commun.*, **512**(4), 921 – 926 (2019).